Magnetic interactions in iron



1992 J. Phys.: Condens. Matter 4 7919

(http://iopscience.iop.org/0953-8984/4/39/007)

J. Phys.: Condens. Matter 4 (1992) 7919–7926. Printed in the UK

# Magnetic interactions in iron

M E Elzain

Department of Physics, College of Science, PO Box 32486, Sultan Qaboos University, Sultanate of Oman

Received 24 April 1992

**Abstract.** A first-principles discrete variational method in the local density approximation is used to calculate the local properties at Fe sites in Fe[$N$, $M$] clusters representing $\alpha$-iron. Here $N$ and $M$ are the respective numbers of antiferromagnetically coupled Fe atoms at the nearest neighbour (NN) and the next nearest neighbour (NNN) sites of the central atom. The local magnetic moment was found to increase slightly with $N$, reach a maximum and decrease with further $N$ values. A large moment is obtained for $N = 0$ and $M = 6$. The magnitude of the magnetic hyperfine field was found to decrease linearly with increasing $N$ for fixed $M$. The average quantities are also calculated treating the AFM atoms as impurities in the $\alpha$-iron lattice. A model is presented which attempts to understand the coupling of the central atom to its NN and NNN as being accomplished through $T_{2g}$ and $E_g$ states respectively.

## 1. Introduction

The interaction between electrons is essential for understanding the properties of transition metals. In particular, magnetism in the 3d metals is a direct consequence of this interaction. For a single isolated atom, Hund's rules lead through the residual Coulomb interaction to the existence of magnetic moments for unfilled shells. When a solid is formed the interatomic interaction between the 3d electrons produces a narrow d band that overlaps the broad sp band. Depending on the number of d electrons, the interatomic distances and the crystal structure, the split magnetic states can be maintained or destroyed [1]. At equilibrium lattice distances the d electrons are classified into itinerant and localized components [2].

In BCC metals the 3d states are hybridized such that those with $T_{2g}$ symmetry are oriented towards nearest neighbour atoms while the states possessing $E_g$ symmetry point towards next nearest neighbours [3]. Because of their interatomic distances the $T_{2g}$ and $E_g$ electrons in iron are considered as itinerant and localized respectively [2]. The $T_{2g}$ electrons form strong d–d bonding whereas the $E_g$ electron bonds are relatively weaker.

The temperature-dependent properties of iron metal exhibit local magnetic-moment characteristics. This is shown by the magnetic susceptibility, which follows the Curie–Weiss law, the spin disorder resistivity and the quasi-elastic magnetic diffuse neutron scattering [4]. The nature of the stable coupling between the local magnetic moments through itinerant d electrons is in general strongly dependent on the number of the latter electrons, as proposed by Stearn [5]. This number is such that the stable coupling in iron is ferromagnetic. Furthermore, it is known that the local magnetic moments are retained well beyond the Curie temperature. At such temperatures the

0953-8984/92/017919+08$04.50  

Fe–Fe couplings are no longer ferromagnetic, in general. However, the amount of short range present is unknown [6].

The average local moment at the Fe site decreases with temperature and vanishes at the Curie point. The magnetic hyperfine field at the Fe site was found to follow this very closely [7]. The timescales of these measurements are very different. Magnetization measurements are on relatively large samples and long timescales, while the hyperfine field measurements are on single sites and timescales of the order of nanoseconds. Thus the rate of change of orientation of the local moment could not be the only reason behind the decrease of the two quantities with temperature.

Peng and Jansen [8] have calculated the exchange constant between Fe–Fe atoms in the ferromagnetic state and in different antiferromagnetic configurations using the full potential linearized augmented plane-wave method. This led to a model Hamiltonian from which the Curie temperature is predicted.

Our objective in this paper is to calculate the local magnetic moment and the magnetic hyperfine field at Fe sites against the antiferromagnetic coupling to nearest and next nearest neighbours. Furthermore, we attempt to understand these results on the basis of chemical bonding and magnetic splitting of the electrons.

The plan of this paper is as follows. In the following section we give an outline of the calculational method used. In section 3 we present and discuss our results. In the last section some concluding remarks are given.

## 2. Calculational model

We took 15-atom clusters as representing the BCC $\alpha$-iron metal. A cluster is denoted by Fe$[N, M]$, where $N$ and $M$ are the number of antiferromagnetically (AFM) coupled Fe atoms in the nearest neighbour (NN) and next nearest neighbour (NNN) shells respectively.

The discrete variational method ([9] and references therein) in the spin-polarized local-density approximation was used to calculate the eigenstates of the Kohn–Sham equation with the von Barth–Hedin exchange-correlation potential. A self-consistent calculation was performed using, as a variational basis, a linear combination of atomic orbitals 3d, 4s and 4p, while the core states were kept frozen. The matrix elements of the Hamiltonian and overlap matrices were obtained by numerical integration. The pseudorandom Diophantine integration method was augmented as desired by a special integration scheme in a spherical volume about particular atoms. Average properties such as atomic configuration, energy levels and magnetic moments converged rapidly with the Diophantine sample, with 300–400 points per atom being sufficient to determine such properties to better than experimental precision. Properties such as contact spin and charge densities, which depend sensitively upon the wavefunction in the atomic core region, require a more careful solution of the Kohn–Sham equation in the region of the probe nucleus. In this region the Diophantine points were replaced by a dense regular (angular $\times$ Gaussian quadrature) mesh.

To calculate the potential the total charge density was cast in a multicentre overlapping multipolar form [10]. The radial density basis set was constructed from spherical atomic densities, calculated from the wavefunction variational basis and from seven parabolic radial functions for each $l = 0$ in the fully symmetric representation of the molecular point group.

Different magnetic configurations were obtained through a selection of relevant initial magnetic moment inputs. The cluster approach offers flexibility in studying

the effect of the surrounding atoms on the central atom up to one at a time. It is not limited by any symmetry requirement such as a unit cell. Furthermore, it is possible to change the interatomic distance of each group of atoms at will. However, it introduces surface effects which might be serious in the case of non-local properties. For local properties it gives reasonable values.

## 3. Results and discussion

The local magnetic moments and the occupation numbers at the central Fe atom presented here were obtained using Mulliken population analysis. We divide the results into two parts. In the first part the $O_h$ point group is used in the symmetrization of the molecular orbitals. This leads directly to the $T_{2g}$ and $E_g$ d occupations and magnetic moments. A model to understand the Fe–Fe d bonding and coupling is subsequently introduced. In the second part the $C_{2v}$ point group is used and the changes in the local magnetic moment and hyperfine field against $N$ and $M$ are presented and discussed.

### *3.1. Bonding and coupling processes*

Table 1 shows the occupation numbers and magnetic moment of the $E_g$ and $T_{2g}$ d states at the central Fe atom for the clusters Fe[PAR], Fe[0, 0], Fe[8, 0], Fe[0, 6] and Fe[8, 6]. The total magnetic moment including the sp contribution is also included. We note that the local d magnetic moment decreased by about 0.3 $\mu_B$ when the coupling to NN was AFM while it increased by the same amount for AFM coupling to NNN. Such trends, however, with a larger decrease and smaller increase, were also obtained by Peng and Jansen [8]. On the other hand the total magnetic moment $\mu_{tot}$ does not decrease and instead it is always greater than the FM coupled clusters. Another feature exhibited by table 1 is the almost constancy of $n_{E_g\uparrow}$ at about a value of 2.0 whereas the other occupations depend on $N$ and $M$. The spin-up states in Fe[0, 0] have a total occupation of 4.63, which is close to the spin-up band occupation obtained with other band methods [11]. We note also that $\mu_{E_g}$ for Fe[0, 0] is larger than 40% of the total moment expected by spherical symmetry, in agreement with experimental results [12].

**Table 1.** The $E_g$ occupations ($n_{E_g\uparrow}$, $n_{E_g\downarrow}$), the $T_{2g}$ occupations ($n_{T_{2g}\uparrow}$, $n_{T_{2g}\downarrow}$), the $E_g$ magnetic moment ($\mu_{E_g}$) in Bohr magnetons, the $T_{2g}$ magnetic moment ($\mu_{T_{2g}}$), the total d moment $\mu_{dtot}$, and the total moment ($\mu_{tot}$) at the central Fe atom in the paramagnetic iron Fe[PAR] and Fe[$N$, $M$] configurations.

| | Fe[PAR] | Fe[0, 0] | Fe[8, 0] | Fe[0, 6] | Fe[8, 6] |
|---|---|---|---|---|---|
| $n_{E_g\uparrow}$ | 1.37 | 1.96 | 1.98 | 1.84 | 1.98 |
| $n_{E_g\downarrow}$ | 1.37 | 0.60 | 1.16 | 0.48 | 0.76 |
| $n_{T_{2g}\uparrow}$ | 2.07 | 2.67 | 2.46 | 2.88 | 2.55 |
| $n_{T_{2g}\downarrow}$ | 2.07 | 1.68 | 1.26 | 1.56 | 1.65 |
| $\mu_{E_g}$ | 0.00 | 1.36 | 0.82 | 1.36 | 1.22 |
| $\mu_{T_{2g}}$ | 0.00 | 0.99 | 1.20 | 1.32 | 0.90 |
| $\mu_{dtot}$ | 0.00 | 2.35 | 2.02 | 2.68 | 2.12 |
| $\mu_{tot}$ | 0.00 | 2.17 | 2.21 | 2.56 | 2.39 |

Energy bands in solids originate from the corresponding atomic levels. In particular the 3d bands are narrow and carry most of the features of the atomic levels implying that orbital overlaps are rather limited to a few shells around each atom. Thus the magnetic structure can in principle be deduced from the bonding of an atom to its NN and NNN atoms. The $T_{2g}$ and $E_g$ states in the BCC lattice have spatial orientations towards the NN and NNN atoms respectively [3]. We assume d bonding such that the central atom bonds to NN through the $T_{2g}$ electrons and to the NNN atoms through the $E_g$ electrons, independent of sp bonding or sd mixing. This d bonding is mainly of the $\sigma$ type. Since the NN distance is smaller than the NNN distance the $T_{2g}$ bonding will be stronger than the corresponding $E_g$ bonding. Such an approach has been used to describe the magnetic structure of BCC iron–phosphorous alloys [13].

For iron in the paramagnetic state (iron with unsplit bands) the d states split into bonding and antibonding parts as shown in figure 1. The $E_g$ levels can take up to two electrons per atom, while the $T_{2g}$ take three electrons. According to the result of Fe[PAR] shown in table 1, two of the $E_g$ electrons go into the $\sigma$ bond and the rest into the $\sigma^*$ bond. Similarly, for the $T_{2g}$ electrons the occupation is as shown in figure 1.

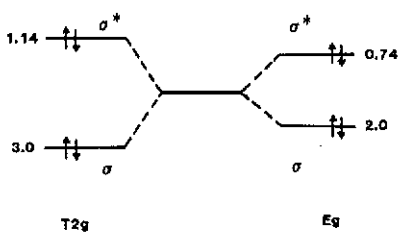


**Figure 1.** The bonding scheme for paramagnetic (magnetically unsplit) iron showing the $T_{2g}$ and the $E_g$ states and their electronic occupation.

Intra-atomic exchange interactions split each of these levels, while the interatomic exchange may enhance or diminish this splitting. When the coupling to both NN and NNN atoms is FM the splitting is enhanced and the local energy states split as shown in figure 2(*a*), with occupations consistent with the results of the Fe[0, 0] cluster.

Antiferromagnetic coupling between the central atom and the NN atoms directly affects the $T_{2g}$ electrons. In this case the $T_{2g}$ splitting diminishes. The energy of the $T_{2g}(\sigma^*)$ spin-up state is increased and electrons are transferred from this state to the $E_g$ states. Furthermore, since the majority electrons at the central atom are pointing up while those at the NN atoms are pointing down then bonding $T_{2g}$ states should reflect this. The sharing of these spin-polarized electrons between the atoms is unequal. Assuming about 0.5 electrons are transferred in each direction to keep charge neutrality, the occupation of these levels is as shown in figure 2(*b*). It is interesting to note that in this case $\mu_{T_{2g}}$ increases because of the increased (decreased) polarization of the full bonding spin-up (spin-down) states. The term $\mu_{E_g}$ decreases since the gained electrons occupy the spin-down states because the spin-up states are already full.

When the NNN atoms are AFM coupled to the central atom the $E_g$ electrons are directly affected and their splitting decreases. Since the spin-up $E_g(\sigma^*)$ are raised in energy, electrons are transferred from this state to the $T_{2g}(\sigma^*)$ spin-up state. The loss of spin-up $E_g(\sigma^*)$ electrons acts to decrease $\mu_{E_g}$. However, polarization of the full bonding $E_g$ electrons similar to that of the full bonding $T_{2g}$ electrons in the case Fe[8, 0] leads to increase in the bonding $E_g$ moment. The net $\mu_{E_g}$ remain effectively unchanged. The NNN atoms also couple AFM to the NN atoms through the $T_{2g}$ electrons,

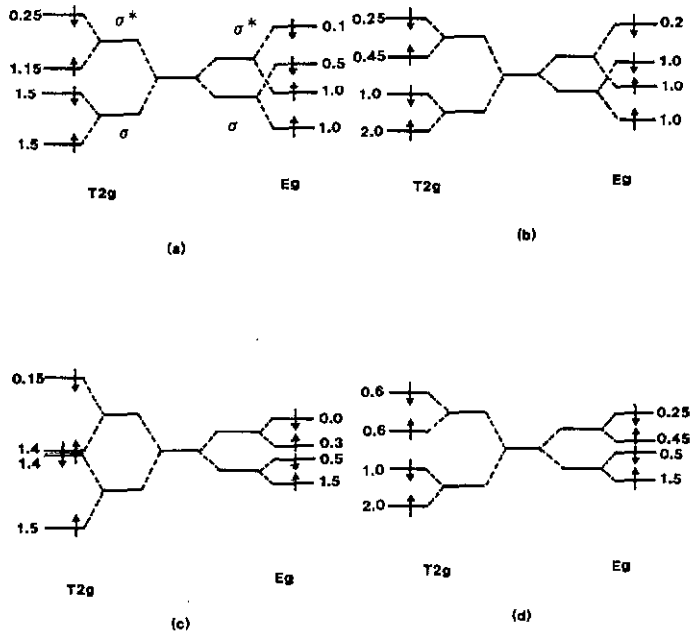


**Figure 2.** The bonding schemes for magnetic iron. (*a*) is the bonding scheme when both NN and NNN Fe atoms are ferromagnetically (FM) coupled to the central atom; (*b*) is when NN are antiferromagnetically (AFM) coupled and NNN are FM. In (*c*) NN are FM coupled and NNN are AFM whereas (*d*) shows the bonding scheme when both NN and NNN are AFM.

increasing the NN $T_{2g}$ moment and hence indirectly affecting the $T_{2g}$ electrons of the central atom. This indirect effect enhances the FM $T_{2g}$ coupling between the central atoms and NN atoms. The resulting energy diagram is as shown in figure 2(*c*). The electrons transferred from the $E_g(\sigma^*)$ spin-up state mainly occupy the $T_{2g}(\sigma^*)$ spin-up state and hence increase $\mu_{T_{2g}}$. Since $\mu_{E_g}$ is unchanged the net result is an increase in the total magnetic moment. This is observed from the results of the Fe[0, 6] cluster.

Antiferromagnetic coupling to both NN and NNN atoms should in principle keep the central-atom moment approximately constant, since in this case no charge transfer between the $E_g$ and $T_{2g}$ states is expected. Both splittings are expected to decrease and both full bonding states are to be polarized. Instead of the electrons being interchanged between the $T_{2g}(\sigma^*)$ spin-up and $E_g(\sigma^*)$ spin-up states they are transferred to the corresponding spin-down antibonding states of the same type. Figure 2(*d*) shows the schematic energy diagram.

To further investigate the validity of such bonding structure we considered two additional cases. In the first case we placed He atoms at the NN and the NNN sites at large interatomic distances. The bonding between Fe and He atoms should be very weak because a He atom has a very deep energy, and furthermore the interatomic spacing we used was very large. Thus, due to the weak coupling between Fe and He, the $T_{2g}$ and $E_g$ states at the Fe central atom are slightly pushed up or remain unchanged. If we think of the Fe–He orbitals as forming bonding and antibonding combinations then the antibonding part is retained by the Fe. The bonding part is occupied by the He. For the cluster Fe[He, Fe], with He positions along the (111)

diagonals and Fe at NNN positions we have $\mu_{T_{2g}} \simeq 2.1\mu_B$ and $\mu_{E_g} \simeq 0.9\mu_B$. In this case the $T_{2g}$ antibonding state is split by the intra-atomic exchange interaction and the spin-up component is nearly full ($\simeq 2.97$ electrons) while the spin-down part has about $\simeq 0.85$ electrons. The $E_g$ state gains some electrons from the states with $T_{2g}$ symmetry, leading to a reduction of the $E_g$ magnetic moment. When the He atoms are placed along the principal axis (100) the results for the cluster Fe[Fe, He] give $\mu_{T_{2g}} \simeq 1$ and $\mu_{E_g} \simeq 1.3$, which are close to the values obtained for Fe[0, 0]. Here the $E_g$ antibonding spin-up states are nearly full ($\simeq 1.9$ electrons) and the spin-down states have about 0.6 electrons. The $T_{2g}$ occupation is also unchanged.

In the other set of calculations we have retained the Fe atomic positions along the (111) and (100) directions but changed the interatomic distances. When the NN are displaced away, so that the distance to the central atom is increased such that it is equal to that of the NNN atoms, we obtain $\mu_{T_{2g}} \simeq 1.7\mu_B$ and $\mu_{E_g} \simeq 1.1\mu_B$. At such distances we expect the bonding between the $T_{2g}$ electrons to decrease and the level splitting becomes similar to that of the $E_g$ electrons. Then both the $\sigma$ and $\sigma^*$ spin-up levels are full ($\simeq 2.9$ electrons) and the spin-down levels are partially occupied ($\simeq 1.2$ electrons), giving a large $\mu_{T_{2g}}$ moment. The change in the $E_g$ moment is relatively small.

On the other hand, when the NNN atoms are displaced towards the central atom by about 0.42 au from 5.42 au to 5.00 au, the $E_g$ bonding increases and the split $\sigma$ and $\sigma^*$ $E_g$ levels no longer overlap. This is similar to the $T_{2g}$ bonding at the equilibrium lattice constant. Thus in this case the $E_g$ moment decreases. We found that $\mu_{E_g} = 0.86\mu_B$. However, $\mu_{T_{2g}} (\simeq 0.72\mu_B)$ also decreases slightly because of the closer NN and NNN interatomic distance which indirectly affects the $T_{2g}$ occupation.

### *3.2. Magnetic hyperfine field*

The magnetic hyperfine field $B_{hf}$ is calculated from the phenomenological relation proposed by Elzain *et al* [14], where the contributions to $B_{hf}$ are divided into valence and core parts. The valence contribution is directly calculated from the self-consistent solution of the Kohn–Sham equation whereas the core contribution is assumed to scale linearly with the local 3d moment, $\mu_d$.

As observed in section 3.1 there are two effects which contribute to changes in $\mu_d$. For fixed $M$ the $\mu_{T_{2g}}$ component increases with increasing N due to the polarization of full bonding $T_{2g}$ states while the $\mu_{E_g}$ component decreases due to conversion of electrons from $T_{2g}$ to $E_g$ symmetry. In figure 3 we show the variation of $\mu_d$ against $N$ for $M$ values fixed at 0 and 4. We note that the two effects act in such a way to give a maxima at around $N = 4$ and beyond this the decrease in $\mu_{E_g}$ dominates the changes in $\mu_d$.

The core contribution to $B_{hf}$ is expected to follow the same pattern as that of $\mu_d$ shown in figure 3. However, when the valence contribution is included the total $B_{hf}$ shows an almost linear variation against $N$. This is shown in figure 4, for some representative clusters having $M = 0$ and $M = 4$. Consequently, the valence contribution plays a major role in the reduction of $B_{hf}$ against changes in the magnetic coupling. Thus, independent of the flipping rate of the local moment, the hyperfine field should decrease due to the positive valence contribution.

The average local and total moments per atom $\bar{\mu}_{Fe}$ and $\bar{\mu}$ respectively and the average hyperfine field $\bar{B}_{hf}$ are also calculated. These averages are obtained by treating the iron atoms with negative moment as impurities in the ferromagnetic iron

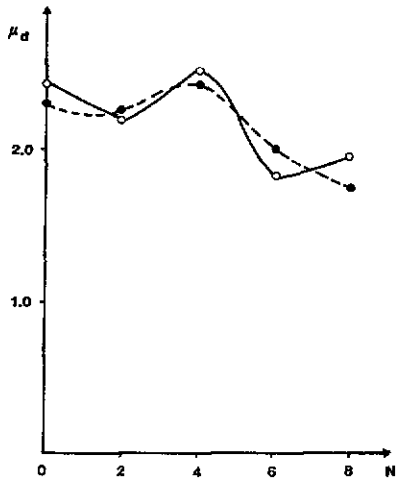


**Figure 3.** The local 3d moment $\mu_d$ at the Fe central site against $N$ for $M = 0$ (full circles) and $M = 4$ (open circles). The curves are for guiding the eye.

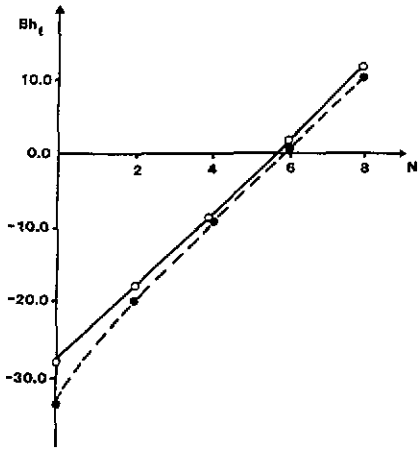


**Figure 4.** The magnetic hyperfine field $B_{hf}$ at the central Fe site against $N$ for $M = 0$ (full circles) and $M = 4$ (open circles). The curves are for guiding the eye.

lattice. The concentration of these atoms is denoted by $c$. The site occupations are given by a random binomial distribution. Figure 5 shows the variation of the scaled $\bar{\mu}_{Fe}$, $\bar{\mu}$ and $\bar{B}_{hf}$ against $c$. We note that $\bar{\mu}_{Fe}$ remains almost constant at the completely ferromagnetic iron value. However, both $\bar{\mu}$ and $\bar{B}_{hf}$ decrease with increasing $c$. For values of $c$ up to about 0.2 the two quantities have an identical variation. Above this concentration $\bar{B}_{hf}$ decreases slower than $\bar{\mu}$. We assume that the concentration $c$ increases with temperature. Hence, if the positive valence contribution is the only reason behind the reduction in $B_{hf}$ then at high temperatures the plot of $B_{hf}$ against temperature will deviate from that of $\bar{\mu}$. However, at high temperatures the flipping rate of the local moment is large and this leads to an additional reduction in $B_{hf}$. The two effects combine together to bring the variation of $B_{hf}$ back in phase with that of $\bar{\mu}$.

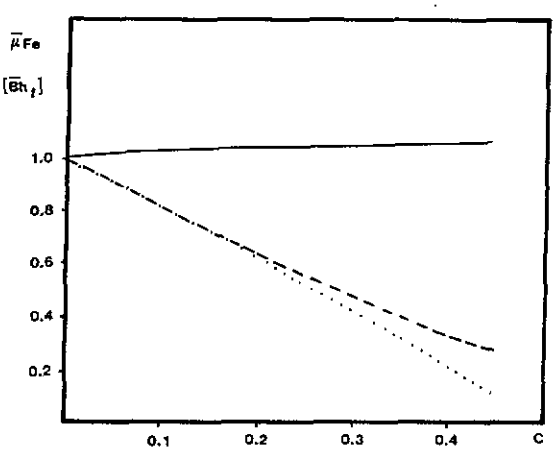


**Figure 5.** The average local magnetic moment at Fe central site $\bar{\mu}_{Fe}$ (full curve), the average total moment per Fe atom $\bar{\mu}$ (dotted curve) and the average magnetic hyperfine field $\bar{B}_{hf}$ (broken curve). These quantities are plotted against the average number of AFM Fe atoms $c$ and each is scaled by the corresponding Fe[0, 0] quantity.

## 4. Conclusion

A first-principles discrete variational method has been used to calculate the local properties at the Fe site in 15-atom clusters representing $\alpha$-iron. The computation has been performed for clusters with different magnetic configurations. It was found that the local magnetic moment changes slightly with changes in the magnetic coupling. In particular, the local moment does not vanish when NN atoms are antiferromagnetically coupled to the central atom. Furthermore, the local moment increases when the coupling of the central atom to its NNN is AFM.

It is conjectured that the magnetic interactions can be understood in terms of a model which takes the coupling to NN atoms to be through the $T_{2g}$ states and that the coupling to NNN atoms to be via $E_g$ states. AFM coupling between the central atom and its nearest neighbour leads to an increase of $\mu_{T_{2g}}$ because of the polarization of the full bonding states while it decreases $\mu_{E_g}$ due to the intra-atomic charge transfer. The increase in the magnetic moment observed for AFM coupled NNN was also explained using the same model.

The local magnetic moment and hyperfine field at the Fe site were also calculated as a function of $N$ and $M$, the number of AFM, NN and NNN atoms respectively. It was found that the magnetic moment at fixed $M$ increases with $N$, reaching its maximum at $N \approx 4$ and decreases with further $N$ values. The magnitude of the magnetic hyperfine field was found to decrease linearly with increasing $N$. The main reason behind this reduction is the positive valence contribution from the AFM coupling.

The averages of the local moment $\bar{\mu}_{Fe}$, the total moment $\bar{\mu}$ and the hyperfine field $\bar{B}_{hf}$ were calculated by treating the relative number of the AFM coupled atoms to be identical to the concentration of impurities in the $\alpha$-iron lattice. It was found that $\bar{\mu}_{Fe}$ retains a constant value while $\bar{\mu}$ and $\bar{B}_{hf}$ decrease linearly with the concentration of the AFM coupled atoms. The variations of $\bar{\mu}$ and $\bar{B}_{hf}$ are similar at low concentrations and they deviate as the concentration increases, with $\bar{B}_{hf}$ having the slower rate. It is suggested that at low temperatures the positive valence contribution is the main reason for the reduction of $B_{hf}$ with temperature. At high temperatures the increase in the flipping rate of the local moment enters as an additional factor. Both effects acting together lead to the variation of $B_{hf}$ with temperature following those of $\mu$.

## References


[1] Moruzzi V L and Marcus P M 1988 *Phys. Rev.* B **38** 1613
[2] Goodenough J B 1963 *Magnetism and the Chemical Bond* (New York: Wiley)
[3] Morinaga M, Yukawa N and Adachi H 1985 *J. Phys. F: Met. Phys.* **15** 1071
[4] Gautier F 1982 *Magnetism of Metals and Alloys* ed M Cyrot (Amsterdam: North-Holland) p 1
[5] Stearn M B 1976 *Phys. Rev.* B **13** 1183
[6] Shirane G, Boni P and Wicksted J P 1986 *Phys. Rev.* B **33** 1881
Lynn J W 1984 *Phys. Rev. Lett.* **52** 775
[7] Preston R S, Hanna S S and Heberle J 1962 *Phys. Rev.* **128** 2207
[8] Peng S S and Jansen H J 1991 *Phys. Rev.* B **43** 3518
[9] Averill F W and Ellis D E 1973 *J. Chem. Phys.* **59** 6412
[10] Delly B and Ellis D E 1982 *J. Chem. Phys.* **76** 1949
[11] Callaway J and Wang C S 1977 *Phys. Rev.* B **16** 2095
Duff K J and Das T P 1971 *Phys. Rev.* B **3** 192
[12] Frollani G, Menzinger F and Sacchetti F 1975 *Phys. Rev.* B **11** 2030
[13] Elzain M E 1991 *Physica* B **173** 251
[14] Elzain M E, Ellis D E and Guenzburger D 1986 *Phys. Rev.* B **34** 1430